Human Erythrocyte-Like Transformation of Synthetic Polymer Vesicles

Eri Yoshida (yoshida.eri.gu@tut.jp)
Toyohashi University of Technology

Research Article

Keywords: human erythrocyte-like transformation, synthetic polymer vesicles, temperature, electron microscopy, spherical vesicles

Posted Date: August 19th, 2021

DOI: https://doi.org/10.21203/rs.3.rs-820861/v1

Scientific Reports, ORIGINAL RESEARCH

Human erythrocyte-like transformation of synthetic polymer vesicles

Eri Yoshida

Department of Applied Chemistry and Life Science, Toyohashi University of Technology

1-1 Hibarigaoka, Tempaku-cho, Toyohashi, Aichi 441-8580, Japan

E-mail: yoshida.eri.gu@tut.jp

Phone & Fax: +81-532-81-5120

Abstract

This paper describes that synthetic polymer vesicles undergo a human erythrocyte-like transformation in response to temperature changes. The normally biconcave discoid erythrocytes, i.e., the discocytes, are transformed into various shapes by their environmental stresses. Field emission scanning electron microscopy (FE-SEM) demonstrates that the spherical vesicles consisting of poly(methacrylic acid)-*block*-poly(*n*-butyl methacrylate-*random*-methacrylic acid), **PMAA-*b*-P(BMA-*r*-MAA)**, transform into echinocyte-like crenate vesicles due to expansion by the component copolymers in being freed from the vesicle surface when heated in an aqueous methanol solution. An increase in the vesicle concentration transforms the spherical vesicles into stomatocyte-like cup-shaped vesicles via the membrane perforation or double invaginations followed by membrane coupling and fusion. Light scattering studies reveal the reversibility and repeatability of the transformations. These findings indicate that the erythrocyte transformations are attributed to the inherent property of the bilayer membrane. The polymer vesicles are helpful for a better understanding of the biomembrane.

Introduction

Human erythrocytes, which play an essential role in respiration as oxygen transporters, have attracted considerable attention from scientists and engineers as a target of artificial creation because of the structural simplicity of the cells that lack a nucleus and other intracellular organelles[1]. A great number of studies about the erythrocytes has been performed from the various aspects of morphological[2-4], rheological[5], biological[6], and pathological investigations[7,8]. The erythrocytes normally have a biconcave discoid shape. They transform in response to their environmental stresses into many different shapes, such as the echinocytes, stomatocytes, spherocytes, acanthocytes, triconcave knizocytes, doughnut-like torocytes with a central flat membrane segment, *etc*., and their in-between shapes[9]. The stresses to induce the transformation include temperature[10,11], pH[12], osmosis[13], salt concentration[11], ions, and amphiphiles[10,11,13,14]. The erythrocyte transformation influences the rheological properties of blood in the microcirculation[15] and causes certain types of anemia in living bodies[16]. The transformation in vitro involves a clinical issue in blood storage for transfusions[17]. Many publications have been released concerning the transformation of mammalian erythrocytes into such abnormal shapes for the purpose of elucidating the cause and mechanism. In particular, the transformations from the discocytes into echinocytes, stomatocytes, and spherocytes have been studied in detail under various conditions with different stresses due to their reversibility and easy production of these abnormal shapes in vitro[8,14,18-20].

Synthetic polymer vesicles consisting of poly(methacrylic acid)-*block*-poly(methyl methacrylate-*random*-methacrylic acid) amphiphilic diblock copolymers are artificial biomembrane models of cells and organelles based on the many similarities in their size, structure[21], morphology[22], membrane impermeability[23], and stimuli-responsive behaviors[24]. Unique models have been created employing the vesicles; for instance, the perforated vesicles for the nuclear envelope[25], the villus-like structure for the villi[26], the anastomosed tubular

networks following a fenestrated sheet for the endoplasmic reticulum and Golgi apparatus[27], the segment copolymers incorporated in the vesicle membrane for cholesterols embedded in the biomembrane[28], and a polyelectrolyte that induces the budding separation for the membrane protein for endocytosis[29]. Recently, it has been found that the vesicles consisting of **PMAA-*b*-P(BMA-*r*-MAA)** undergo the erythrocyte-like transformation when heated in an aqueous methanol solution. This paper describes the similarities between the vesicles and erythrocytes during their transformations.

Results

The amphiphilic diblock copolymer of **PMAA-*b*-P(BMA-*r*-MAA)** produces spherocyte I-like[9] spherical vesicles with a dimple by the polymerization-induced self-assembly in a 70% aqueous methanol solution. The dimpled spherical vesicles transformed into echinocyte-like crenate vesicles when heated in the solution ([vesicles] = 5.68g/L). FE-SEM revealed that the crenate vesicles were formed by the outward force of the membrane based on the component copolymers to be freed from the vesicles when heated (Fig. 1a). With the rising temperature, the vesicle surface became rough due to an increase in the molecular motion of the components (Fig. 1bA,B). The vesicles were expanded by the outward force (Fig. 1bC), reached the maximum expansion (Fig. 1bD), then shrank, releasing the microspherules of the copolymers (Fig. 1bE). The microspherules averaged D_n = 125.1 nm in diameter. The vesicles finally transformed into the echninocyte III-like[4,9] vesicles (Fig. 1bF). By cooling, the crenate vesicles along with the microspherules reverted to dimpled and spherical vesicles (Fig. 1bG). This reversible transformation was repeatable, although the excessively repeated operation partly joined the vesicles (Fig. 1bH). Light scattering studies supported the expansion-shrinking mechanism for the transformation. The hydrodynamic size (D_h) of the spherical vesicles was increased by heating, reached a maximum, then decreased (Fig.

2a). By cooling, the D_h reverted to the original size, following the same course. This thermo-responsive hysteresis of the D_h was also reversible and repeatable (Fig. 2b). The variation in the scattering intensity distribution of D_h verified the release of the microspherules from the vesicles at high temperature (Fig. 2c). The distribution of the vesicles was shifted to the higher side by heating, then oppositely shifted to the lower side by further heating. At a much higher temperature, the distribution of the microspherules (D_h = 107.3 nm) was separated from that of the vesicles. By cooling, the distribution reverted back to the original position, tracing the same process.

An increase in the vesicle concentration ([vesicles] = 9.94 g/L) transformed the spherical vesicles into stomatocyte-like cup-shaped vesicles at high temperature. The FE-SEM observations suggested that this transformation involves two different mechanisms (Fig. 3a); one is the principal pathway of a single membrane invagination, followed by perforation at the dimple (Fig. 3bA,B), and the other is a pathway of simultaneous double invaginations on the dimple and its opposite sides, followed by the coupling and fusion of the membranes. This membrane coupling-fusion mechanism was proved by the formation of biconcave discoid vesicles during the process of transformation (Fig. 3bC). A low number of the discoid vesicles at 35°C increased in number with the temperature increase to 40°C; however, they almost disappeared at 45°C. The discoid vesicles were the intermediates during the transformation into cup-shaped vesicles. In addition to the discoid vesicles, a very low number of knizocyte-like vesicles were discerned at 40°C (Fig. 3bD). The knizocyte-like vesicles were also intermediates during the transformation because most of them were not observed over 40°C. At 50°C, all the vesicles transformed into stomatocyte II-like[4,9] vesicles (Fig. 3bE). Keeping the vesicles at this high temperature for 4 h partly transformed the cup-shaped vesicles into torocyte-like vesicles with a target cell appearance (Fig. 3bF). Some of the torocyte-like

vesicles were perforated in their central flat membrane segments (Fig. 3bG) or had a doughnut-like shape (Fig. 3bH). By cooling, the vesicles reverted to the dimpled spherical shape (Fig. 3bI). This transformation into stomatocyte-like vesicles was completely reversible and repeatable based on the light scattering analysis (Fig. 4). A decrease in D_h by the transformation into the cup-shaped vesicles is due to the fact that the lateral movement of the cup-shaped vesicles is preferable more than the vertical movement.

The solvent affinity dominates the shape of the vesicles by the transformation. As a result of increasing the methanol content to 80% in the solution, the spherical vesicles transformed into crenate vesicles along with microspherules even at a high vesicle concentration ([vesicles] = 9.96 g/L) (Fig. 5A). An increase in the solvent affinity enhanced the outward force of the copolymers in being freed from the vesicles. The crenate vesicles returned to dimpled spherical vesicles by cooling (Fig. 5B), as were those in the 70% solution. On the other hand, a decrease in the solvent affinity by lowering the methanol content to 60% increased the number of biconcave discoid vesicles and knizocyte-like vesicles, although most of the transforms were cup-shaped vesicles (Fig. 5C). Some of the vesicles hardly reverted to the spherical vesicles even by cooling and retained their shapes at 25°C (Fig. 5D). By further lowering the content to 50%, not all the vesicles transformed into cup-shaped vesicles even at 50°C (Fig. 5E). The lower solvent affinity produced a slight number of stomato II-acanthocyte-like[9] (Fig. 5F) and torocyte-like vesicles (Fig. 5G) instead of the discocyte- and knizocyte-like vesicles. The shape replacement by decreasing the solvent affinity suggests that the stomato II-acanthocyte-like and torocyte-like vesicles were formed by a decrease in the flexibility of the membrane. A still lower content below 40% prevented the spherical vesicles from transforming and retained their spherical shape even at 50°C (Fig. 5H).

Discussion

The polymer vesicles and the erythrocytes have several similarities in their transformations. The vesicles and erythrocytes transform both reversibly and repeatedly into a crenate or cup shape. The mechanisms of their transformations are also similar. The vesicles undergo an echinocyte-like transformation by the membrane expansion due to the copolymers being freed from the vesicle surface, while the erythrocytes transform into echinocytes, releasing microspherules of the component lipids from the cell surface[30]. Similarly, the transformation into cup-shaped vesicles is caused by the shrinking due to a decrease in a ratio of the internal space volume to the surface area, as is the stomatocytic transformation of the erythrocytes. The vesicles and erythrocytes also have in common that the biconcave discoid shape is the intermediate during the transformation. The knizocyte-, torocyte-, and acanthocyte-like vesicles are other intermediates during the transformation into a cup shape. It has been reported that the torocytes and knizocytes are formed by the stomatocytes losing volume by the membrane invagination while maintaining their surface area[31,32]. The most stable shape both for the vesicles and erythrocytes is spherical when the shape retention of the erythrocytes by the spectrin network[33] is excluded from consideration. The discocytes are transformed into the spherocytes by a spectrin deficiency[34-36]. Furthermore, the vesicles and erythrocytes both have a similar transformation temperature-dependence. Only the difference is that the vesicle transformation is caused at high temperatures both into crenate and cup-shaped vesicles, whereas the erythrocytes undergo the echinocytic transformation at low temperature, although the stomatocytic transformation proceeds at high temperature[11]. These temperature-dependent transformations of the erythrocytes occur only in the specific regions of different pHs and NaCl concentrations. Therefore, it is difficult to simply compare their thermo-responsive transformations since the erythrocyte transformation is dominated by these factors.

For factors to determine the final form of the erythrocytes by the transformation, some

explanations have been provided; one description is based on the bilayer-couple hypothesis, where the final shape is determined by the difference in bending between the inner and outer leaflets of the membrane[19,37]. The difference in bending is considered to be produced in the extremely low area due to inhomogeneities in the plane of the lipid bilayer. As regard to this explanation, Bessis proposed the structural memory effect for the echinocytic transformation based on experimental results demonstrating that the crenation always occurred at the same place in the surface during the repeated transformation and reformation[38]. The vesicles consist of a single component of the diblock copolymer, although it has a distribution in the molecular weight. During the crenation, the copolymers with a relatively low molecular weight are expected to quickly leave the vesicle surface because they have more affinity to the solvent. The erythrocyte membrane is composed of a great number of different kinds of lipids that have their specific shapes and affinity. It is considered that the identical lipids with a high affinity always form crenate in the cell surface during the repeated transformation and that this phenomenon is regarded as the structural memory effect[38,39].

In conclusion, the synthetic polymer vesicles and erythrocytes have much in common regarding their transformations, just because they consist of the bilayer membrane, although their components are quite different in size and ingredients. The findings in this study indicate that the erythrocyte transformations are attributed to the inherent property of the bilayer membrane. This is the first study demonstrating that the non-natural polymer vesicles are helpful for elucidating and better understanding the intrinsic properties and behaviors of the erythrocyte membrane.

Methods

Instrumentation. A Ushio UV irradiation system consisting of an optical modulex BA-H502, an illuminator OPM2-502H with a high-illumination lens UI-OP2SL, and a 500W super high-

pressure UV lamp USH-500SC2 was used for preparing the polymer vesicles by the photopolymerization-induced self-assembly. FE-SEM measurements were performed using a Hitachi SU8000 scanning electron microscope. Light scattering studies were performed by a Photal Otsuka Electronics ELS-8000 electrophoretic light scattering spectrophotometer equipped with a system controller, an ELS controller, and a He-Ne laser operating at λ = 632.8 nm and the angle of θ = 90°. The D_h of the vesicles was estimated by the cumulant analysis, while the scattering intensity distribution was obtained by the Marquardt analysis[40]. ^{1}H NMR measurements were conducted using a Jeol ECS500 FT NMR spectrometer. Gel permeation chromatography (GPC) was performed using a Tosoh GPC-8020 instrument equipped with a DP-8020 dual pump, a CO-8020 column oven, and a RI-8020 refractometer. Two gel columns, Tosoh TSK-GEL α-M were used with *N*,*N*-dimethylformamide containing 30 mM LiBr and 60 mM H_3PO_4 as the eluent at 40°C. The molecular weight and its distribution were estimated by GPC based on **PMAA** standards.

FE-SEM observations. The vesicles were dried in air and subjected to the FE-SEM measurements at 1.0 kV without any coating.

Light scattering measurement. The vesicles were dispersed in an aqueous methanol solution (CH_3OH/H_2O = 3/1 *v*/*v*) by vigorous shaking, then subjected to the light scattering studies.

PMAA-*b*-P(BMA-*r*-MAA) vesicles. The vesicles were prepared as previously reported by the photo controlled/living radical polymerization mediated by 4-methoxy-2,2,6,6-tetramethylpiperidine-1-oxyl (**MTEMPO**)[41]; **MTEMPO** (18.0 mg, 0.0966 mmol), 2,2-azobis[2-(2-imidazolin-2-yl)propane] (22.8 mg, 0.0911 mmol), (4-*tert*-

butylphenyl)diphenylsulfonium triflate (24.0 mg, 0.0512 mmol), methacrylic acid (**MAA**) (2.030 g, 23.6 mmol), and methanol (4 mL) were placed in a test tube connected to a high vacuum valve. The contents were degassed several times using a freeze-pump-thaw cycle and charged with N_2. The polymerization was carried out at room temperature for 5.5 h by irradiation with a 500W high-pressure mercury lamp at 9.0 amperes using the reflective light from a mirror in order to avoid any thermal polymerization caused by the direct irradiation[42]. To the resulting solution were added methanol (11 mL) and distilled water (5 mL) degassed by bubbling Ar for 15 min under a flow of Ar. After the product was completely dissolved in the aqueous methanol, part of the mixture (ca. 1 mL) was withdrawn to determine the monomer conversion and molecular weight of the **PMAA** end-capped with **MTEMPO** (**PMAA-MTEMPO**). The **MAA** conversion was 75.9% by ^{1}H NMR, while the molecular weight and molecular weight distribution of the **PMAA-MTEMPO** were estimated to be M_n = 13,630 and M_w/M_n = 1.711, respectively (see Supplementary Information). The withdrawn solution was poured into ether (50 mL) to precipitate the polymer. The precipitate was collected by filtration and dried in vacuo for several hours to obtain the polymer (60.6 mg). The solution of the **PMAA-MTEMPO** (4 mL containing 0.01933 mmol of the **PMAA-MTEMPO** and 1.137 mmol of unreacted **MAA** based on the **MAA** conversion), **BMA** (563.2 mg, 3.961 mmol), and **MAA** (274.1 mg, 3.183 mmol) were placed in a 30-mL test tube connected to a high vacuum valve under a flow of Ar. The initial molar ratio of the monomers was **BMA**/**MAA** = 0.478/0.522. The contents were degassed several times using a freeze-pump-thaw cycle and finally charged with N_2. The polymerization was carried out for 8 h at room temperature and 600 rpm by irradiation at the current of 9.1 amperes using the reflective light. After the polymerization, part of the resulting dispersion solution (ca. 0.5 mL) was withdrawn using a syringe to determine the conversions. A mixed solvent (CH_3OH/H_2O = 3/1 *v*/*v*, 20 mL) was added to the dispersion solution to precipitate the

vesicles. The vesicles were cleaned with the mixed solvent by a repeated sedimentation-redispersion process. The resulting vesicles were stored in the presence of a small amount of the mixed solvent. The molar ratio of units and degrees of polymerization (DPs) for the blocks were determined to be **PMAA$_{211}$-*b*-P(BMA$_{0.553}$-*r*-MAA$_{0.447}$)$_{287}$** by ^{1}H NMR based on the monomer conversions (77% for **BMA**, 57% for **MAA**, and Supplementary Information). The molecular weight and molecular weight distribution of the copolymer were calculated to be M_n = 49,060 and M_w/M_n = 1.631, respectively (Supplementary Information).

Acknowledgments

This work was supported by the JSPS Grant-in-Aid for Scientific Research (Grant Number 18K04863).

Competing interests

The author has no conflict of interest in this study.

References

1. Guo, J., Agola, J. O., Serda, R., Franco, S., Lei, Q., Wang, L., Minster, J., Croissant, J. G., Butler, K. S., Zhu, W. & Brinker, C. J. Biomimetic rebuilding of multifunctional red blood cells: Modular design using functional components. *ACS Nano* **14**, 7847–7859 (2020).
2. Nakao, M., Nakao, T. & Yamazoe, S. Adenosine triphosphate and maintenance of shape of the human red cells. *Nature* **187,** 945–946 (1960).
3. Rudenko, S. V. Erythrocyte morphological states, phases, transitions and trajectories.

Biochim. Biophys. Acta **1798,** 1767–1778 (2010).

4. Geekiyanage, N. M., Balanant, M. A., Sauret, E., Saha, S., Flower, R., Lim, C. T. & Gu, Y. A coarse-grained red blood cell membrane model to study stomatocyte-discocyte-echinocyte morphologies. *Plos One* **14,** e0215447, 1–25 (2019).
5. Braasch, D. Red cell deformability and capillary blood flow. *Physiol. Rev*. **51,** 679–701 (1971).
6. Elgsaeter, A., Stokke, B. T., Mikkelsen, A. & Branton, D. The molecular basis of erythrocyte shape. *Science* **234,** 1217–1223 (1986).
7. Bessis, M. & Lessin, L. S. The discocyte-echinocyte equilibrium of the normal and pathologic red cell. *Blood* **36,** 399–403 (1970).
8. Weed, R. I. & Bessis, M. The discocyte-stomatocyte equilibrium of normal and pathologic red cells. *Blood* **41**, 471–475 (1973).
9. Bessis, M. Red cell shapes. An illustrated classification and its rationale. *Red Cell Shape* 1–25 (Springer-Verlag, 1973).
10. Glaser, R. The shape of red blood cells as a function of membrane potential and temperature. *J. Membrane Biol*. **51,** 217–228 (1979).
11. Glaser, R. & Donath, J. Temperature and transmembrane potential dependence of shape transformations of human erythrocytes. *Bioelectrochem. Bioenerg*. **27,** 429–440 (1992).
12. Weed, R. I. & Chailley, B. Calcium-pH interactions in the production of shape change in erythrocytes. *Red Cell Shape* 55–68 (Springer-Verlag, 1973).
13. Pfafferott, C., Nashj, G. B. & Meiselman, H. J. Red blood cell deformation in shear flow. Effects of internal and external phase viscosity and of in vivo aging. *Biophys. J.* **47,** 695–704 (1985).
14. Deuticke, B. Transformation and restoration of biconcave shape of human erythrocytes induced by amphiphilic agents and changes of ionic environment. *Biochim. Biophys.*

Acta **163**, 494–500 (1968).

15. Chien, S., Usami, S., Dellenback, R. J. & Gregersen, M. Blood viscosity: Influence of erythrocyte deformation. *Science* **157**, 827–829 (1967).
16. Bull, B. S. & Kuhn, I. N. The production of schistocytes by fibrin strands (A scanning electron microscope study) *Blood* **35,** 104–111 (1970).
17. Haradin, A. R., Weed, R. I. & Reed, C. F. Changes in physical properties of stored erythrocytes. *Transfusion* **9,** 229–237 (1969).
18. Rumsby, M. G., Trotter, J., Allan, D. & Michell, R. H. Recovery of membrane micro-vesicles from human erythrocytes stored for transfusion: A mechanism for the erythrocyte discocyte-to-spherocyte shape transformation. *Biochem. Soc. Trans*. **5,** 126–128 (1977).
19. Sheetz, M. P. & Singer, S. J. Biological membranes as bilayer couples. A molecular mechanism of drug-erythrocyte interactions. *Proc. Nat. Acad. Sci. USA*, **71**, 4457–4461 (1974).
20. Reinhart, W. H. & Chien, S. Echinocyte-stomatocyte transformation and shape control of human red blood cells: Morphological aspects. *Am. J. Hematol*. **24**, 1–14 (1987).
21. Yoshida, E. Giant vesicles prepared by nitroxide-mediated photo-controlled/living radical polymerization-induced self-assembly. *Colloid Polym. Sci*. **291,** 2733–2739 (2013).
22. Yoshida, E. Worm-like vesicle formation by photo-controlled/living radical polymerization-induced self-assembly of amphiphilic poly(methacrylic acid)-*block*-poly(methyl methacrylate-*random*-methacrylic acid). *Colloid Polym. Sci.* **294**, 1857–1863 (2016).
23. Yoshida, E. Enhanced permeability of Rhodamine B into bilayers comprised of amphiphilic random block copolymers by incorporation of ionic segments in the

hydrophobic chains. *Colloid Polym. Sci*. **293**, 2437–2443 (2015).

24. Yoshida, E. PH response behavior of giant vesicles comprised of amphiphilic poly(methacrylic acid)-*block*-poly(methyl methacrylate-*random*-methacrylic acid). *Colloid Polym. Sci*. **293**, 649–653 (2015).
25. Yoshida, E. Perforated giant vesicles composed of amphiphilic diblock copolymer: New artificial biomembrane model of nuclear envelope. *Soft Matter* **15,** 9849–9857 (2019).
26. Yoshida, E. Fabrication of microvillus-like structure by photopolymerization-induced self-assembly of an amphiphilic random block copolymer. *Colloid Polym. Sci*. **293**, 1841–1845 (2015).
27. Yoshida, E. Fabrication of anastomosed tubular networks developed out of fenestrated sheets through thermo responsiveness of polymer giant vesicles. *ChemXpress* **10(1):118**, 1–11 (2017).
28. Yoshida, E. Morphological changes in polymer giant vesicles by intercalation of a segment copolymer as a sterol model in plasma membrane. *Colloid Polym. Sci*. **293**, 1835–1840 (2015).
29. Yoshida, E. Morphology transformation of giant vesicles by a polyelectrolyte for an artificial model of a membrane protein for endocytosis. *Colloid Surf. Sci*. **3(1)**, 6–11 (2018).
30. Bessis, M. & Mandon, P. La microspherulation et les forms myeliniques des globules rouges. Examen compare au microscope electronique a balayage et a transmission. *Nouv. Rev. Fr. Hematol*. **12,** 443–454 (1972).
31. Bobrowska-Hägerstrand, M., Kralj-Iglic, V., Iglic, A., Bialkowska, K., Isomaa, B. & Hägerstrand, H. Torocyte membrane endovesicles induced by octaethyleneglycol dodecylether in human erythrocytes. *Biophys. J*. **77,** 3356–3362 (1999).

32. Zambrano, P., Suwalsky, M., Jemiola-Rzeminska, M. & Strzalka, K. α1-and β-adrenergic antagonist labetalol induces morphological changes in human erythrocytes. *Biochem. Biophys. Res. Commun.* **503,** 209–214 (2018).

33. Byers, T. J. & Branton, D. Visualization of the protein associations in the erythrocyte membrane skeleton. *Proc. Natl. Acad. Sci. USA*, **82**, 6153–6157 (1985).

34. Palek, J. & Lux, S. E. Red cell membrane skeletal defects in hereditary and acquired hemolytic anemias. *Semin. Hematol*. **20**, 189–224 (1983).

35. Goodman, S. R., Shiffer, K. A., Casoria, L. A. & Eyster, M. E. Identification of the molecular defect in the erythrocyte membrane skeleton of some kindreds with hereditary spherocytosis. *Blood* **60**, 772–784 (1982).

36. Ponder, E. The spherical form of the mammalian erythrocyte III. Changes in surface area in disks and spheres. *J. Exp. Biol.* **14,** 267–277 (1937).

37. Sheetz, M. P., Painter, R. G. & Singer S. J. Biological membranes as bilayer couples III. Compensatory shape changes induced n membranes. *J. Cell Biol*. **70**, 193–203 (1976).

38. Bessis, M. & Prenant, M. Topographie de L'apparition des spicules dans les erythrocytes creneles (Echinocytes). *Nouv. Rev. Fr. Hematol*. **13,** 351–364 (1972).

39. Lange, Y. & Slayton, J. M. Interaction of cholesterol and lysophosphatidylcholine in determining red cell shape. *J. Lipid Res*. **23,** 1121–1127 (1982).

40. Marquardt, D. W. An algorithm for least-squares estimation of nonlinear parameters. *J. Soc. Indust. Appl. Math.* **11,** 431–441 (1963).

41. Yoshida, E. Hydrophobic energy estimation for giant vesicle formation by amphiphilic poly(methacrylic acid)-*block*-poly(alkyl methacrylate-*random*-methacrylic acid) random block copolymers. *Colloid Polym. Sci*. **292,** 2555–2561 (2014).

42. Yoshida, E. Effects of illuminance and heat rays on photo-controlled/living radical polymerization mediated by 4-methoxy-2,2,6,6-tetramethylpiperidine-1-oxyl. *ISRN Polym. Sci.* **2012,** 102186, 1-6 (2012).

Figure legends

Figure 1. The echinocyte-like transformation. **a**, A schematic mechanism of the transformation. **b**, FE-SEM images of the vesicles during the echinocyte-like transformation at (**A**-**F**) each temperature by heating, (**G**) 25°C by cooling, and (**H**) 25°C after three repetitions of the heat-to-cool process.

Figure 2. The light scattering analysis of the echinocyte-like transformation. **a,** The variation in D_h of the vesicles by the temperature change. **b,** The D_h change for the repeated heat-to-cool process. **c,** The variation in scattering intensity distribution of D_h by the temperature change. [vesicles] = 5.68g/L

Figure 3. The stomatocyte-like transformation. **a**, Schematic mechanisms of the transformation. **b**, FE-SEM images of the vesicles during the transformation; (**A**) spherocyte-like dimpled spherical vesicles, 25°C, (**B**) for a single invagination, 35°C, (**C**) a discocyte-like vesicle, 35°C, (**D**) a knizocyte-like vesicle, 40°C, (**E**) stomatocyte II-like vesicles, 50°C, (**F**) a torocyte-like vesicle, 50°C, (**G**) a perforated torocyte-like vesicle, 50°C, (**H**) a doughnut-like vesicle, 50°C, and (**I**) dimpled spherical vesicles by cooling, 25°C.

Figure 4. Reversibility and repeatability of the stomatocyte-like transformation. **a,** The thermo-responsive hysteresis of the vesicles. **b,** The variation in scattering intensity distribution of D_h by heating and cooling. **c,** The D_h change for the repeated heat-to-cool process and FE-SEM images of the vesicles after three repetitions of the process. [vesicles] = 9.94 g/L

Figure 5. Effect of the solvent affinity on the transformation. FE-SEM images of the vesicles in the solution with the methanol content of (**A**) 80%, 50°C, (**B**) 80%, 25°C, (**C**) 60%, 50°C, (**D**) a knizocyte-like vesicle, 60%, 25°C, (**E**) 50%, 50°C, (**F**) a stomato II-acanthocyte vesicle, 50%, 50°C, (**G**) a torocyte-like vesicle, 50%, 50°C, (**H**) 40%, 50°C.

Figures

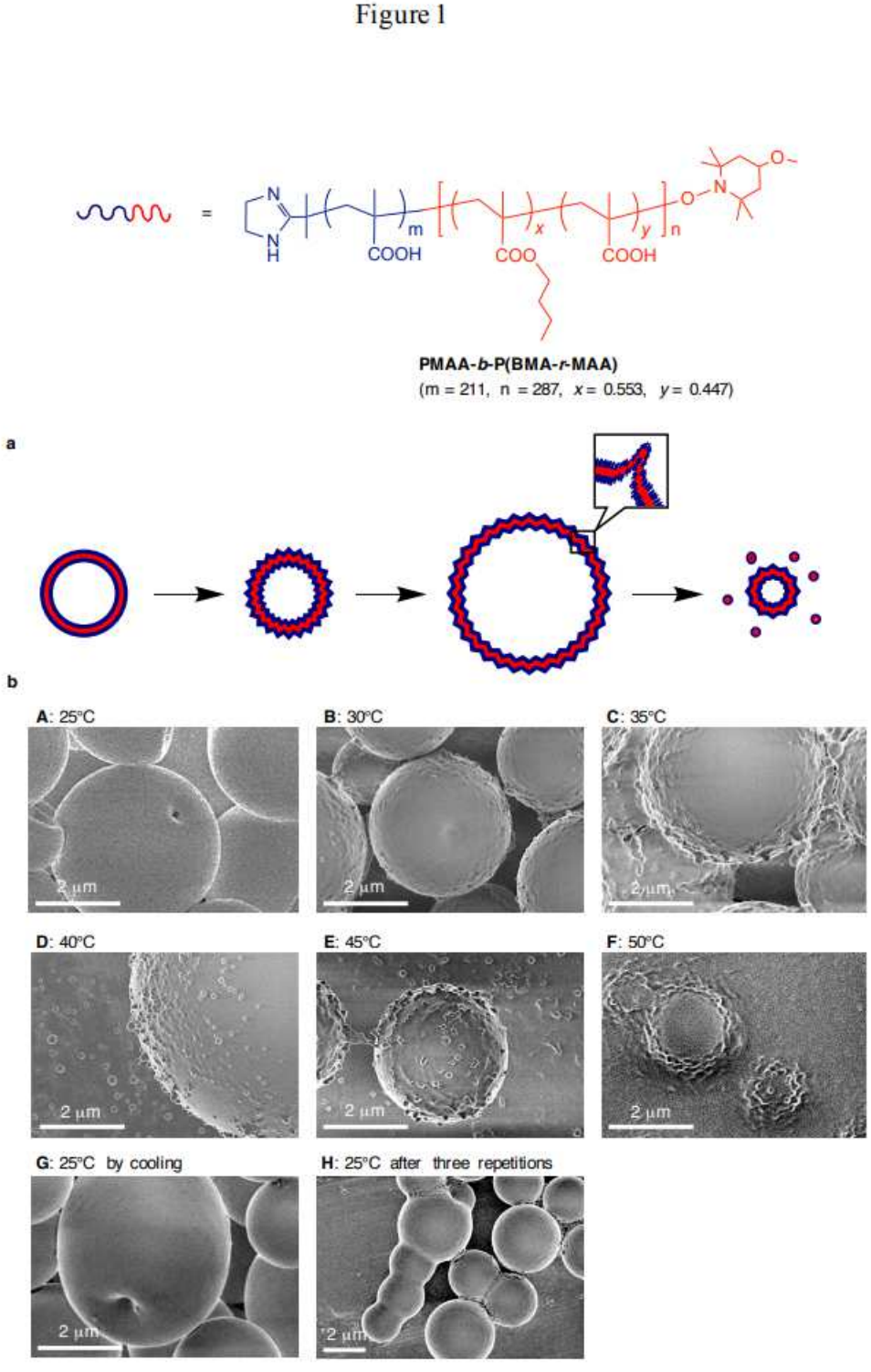

Figure 1

The echinocyte-like transformation. a, A schematic mechanism of the transformation. b, FE-SEM images of the vesicles during the echinocyte-like transformation at (A-F) each temperature by heating, (G) 25°C by cooling, and (H) 25°C after three repetitions of the heat-to-cool process.

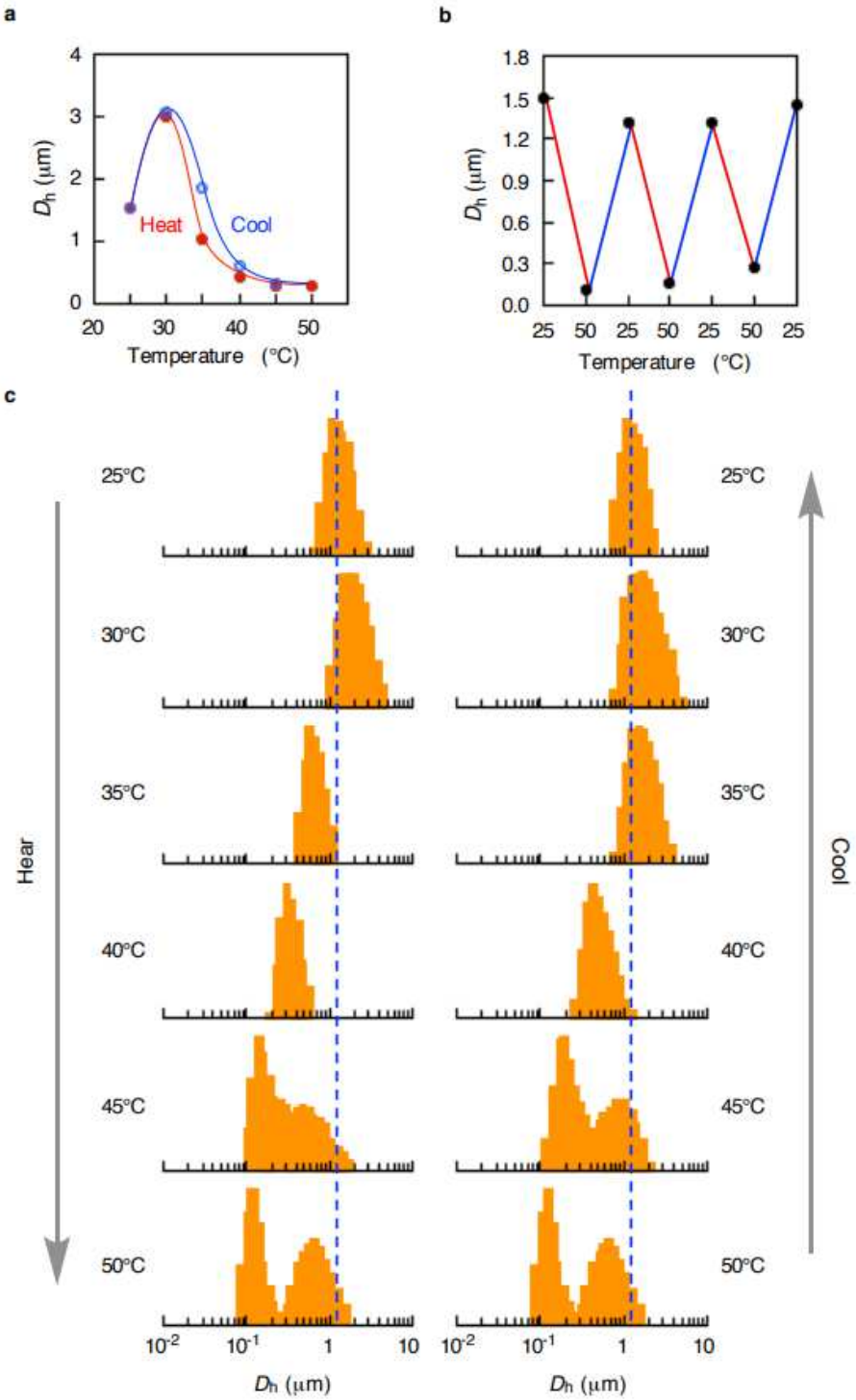

Figure 2

The light scattering analysis of the echinocyte-like transformation. a, The variation in Dh of the vesicles by the temperature change. b, The Dh change for the repeated heat-to-cool process. c, The variation in scattering intensity distribution of Dh by the temperature change. [vesicles] = 5.68g/L

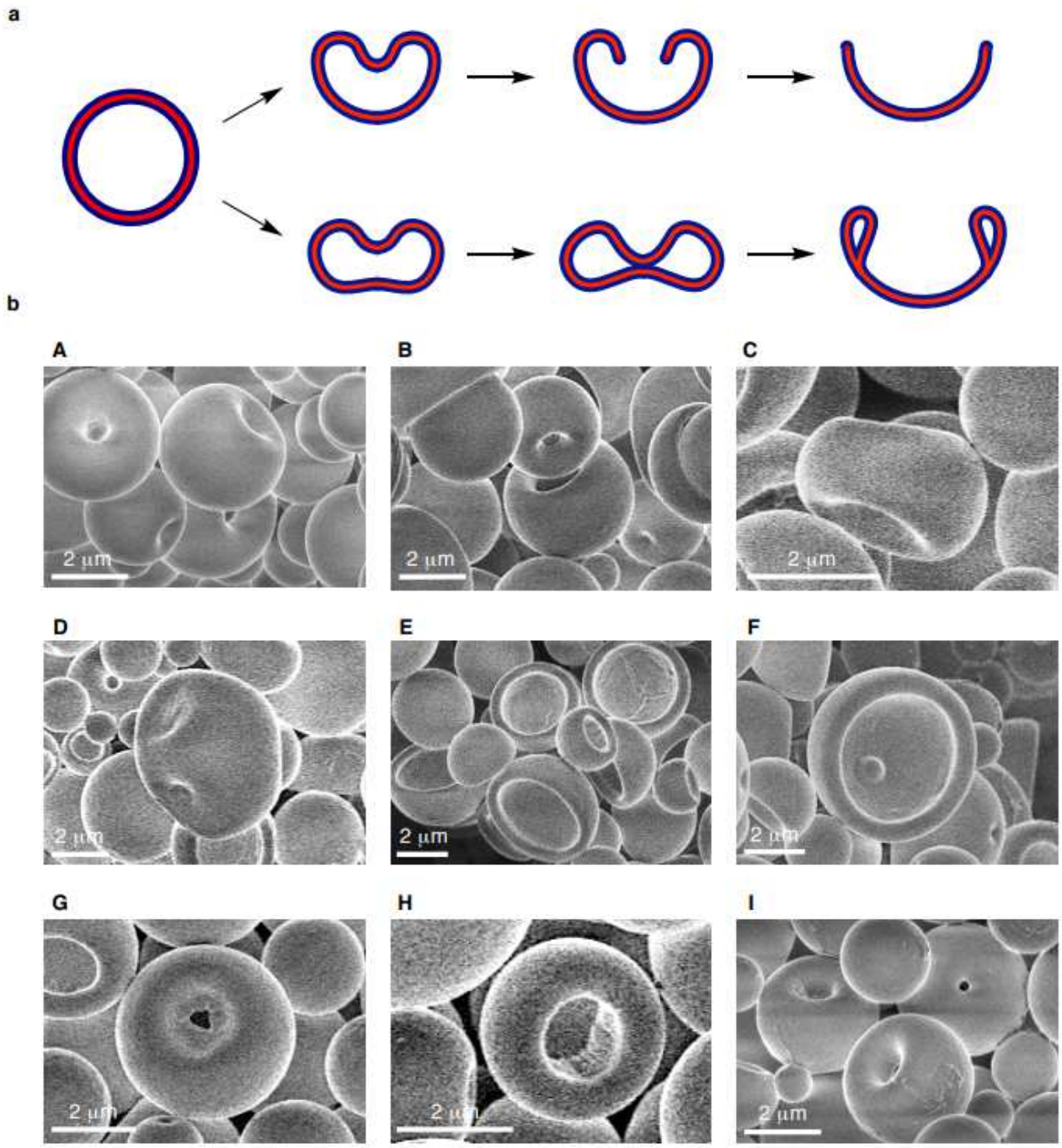

Figure 3

The stomatocyte-like transformation. a, Schematic mechanisms of the transformation. b, FE-SEM images of the vesicles during the transformation; (A) spherocyte-like dimpled spherical vesicles, 25°C, (B) for a single invagination, 35°C, (C) a discocyte-like vesicle, 35°C, (D) a knizocyte-like vesicle, 40°C, (E) stomatocyte II-like vesicles, 50°C, (F) a torocyte-like vesicle, 50°C, (G) a perforated torocyte-like vesicle, 50°C, (H) a doughnut-like vesicle, 50°C, and (I) dimpled spherical vesicles by cooling, 25°C.

Figure 4

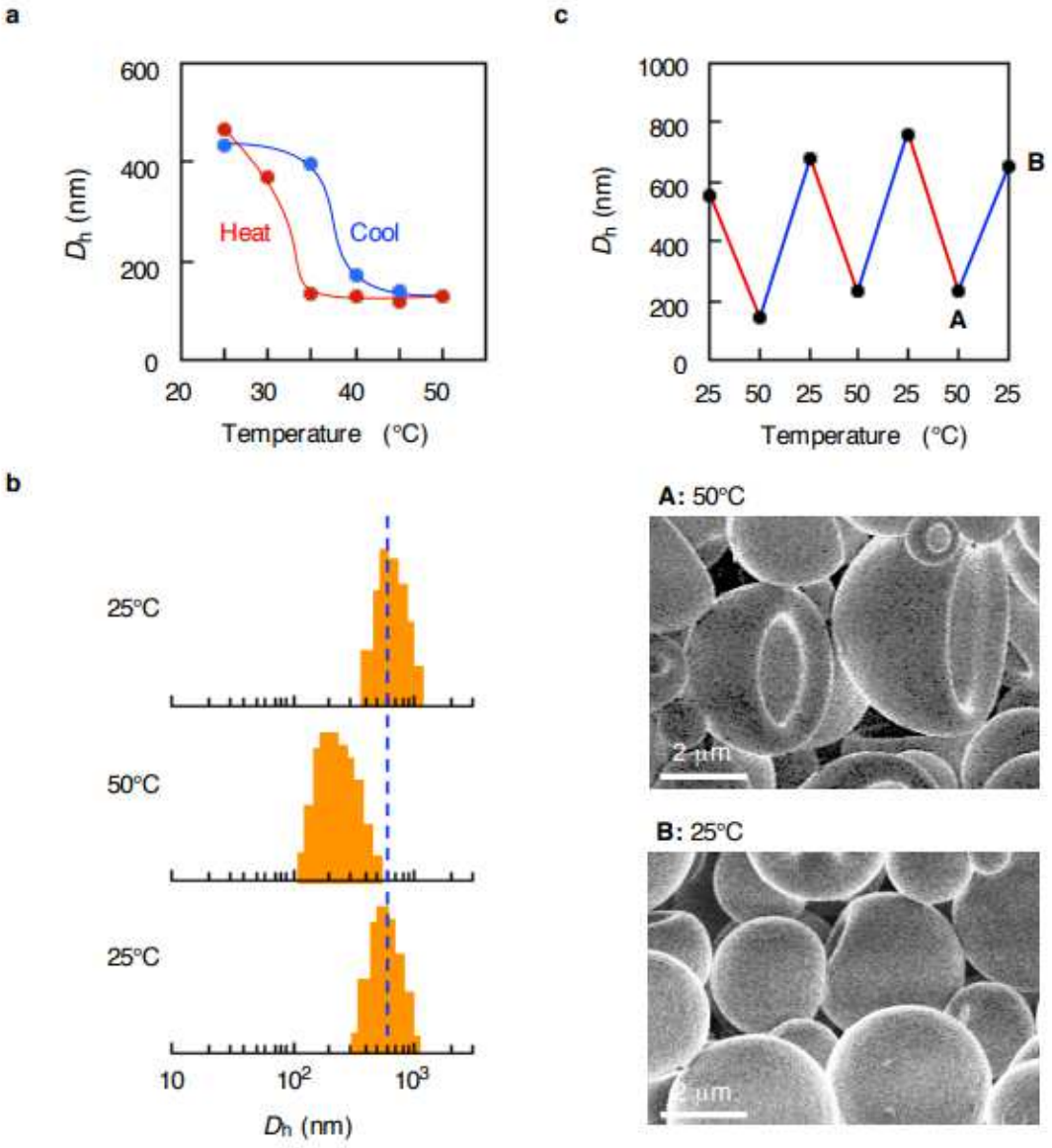

Figure 4

Reversibility and repeatability of the stomatocyte-like transformation. a, The thermo-responsive hysteresis of the vesicles. b, The variation in scattering intensity distribution of Dh by heating and cooling. c, The Dh change for the repeated heat-to-cool process and FE-SEM images of the vesicles after three repetitions of the process. [vesicles] = 9.94 g/L

Figure 5

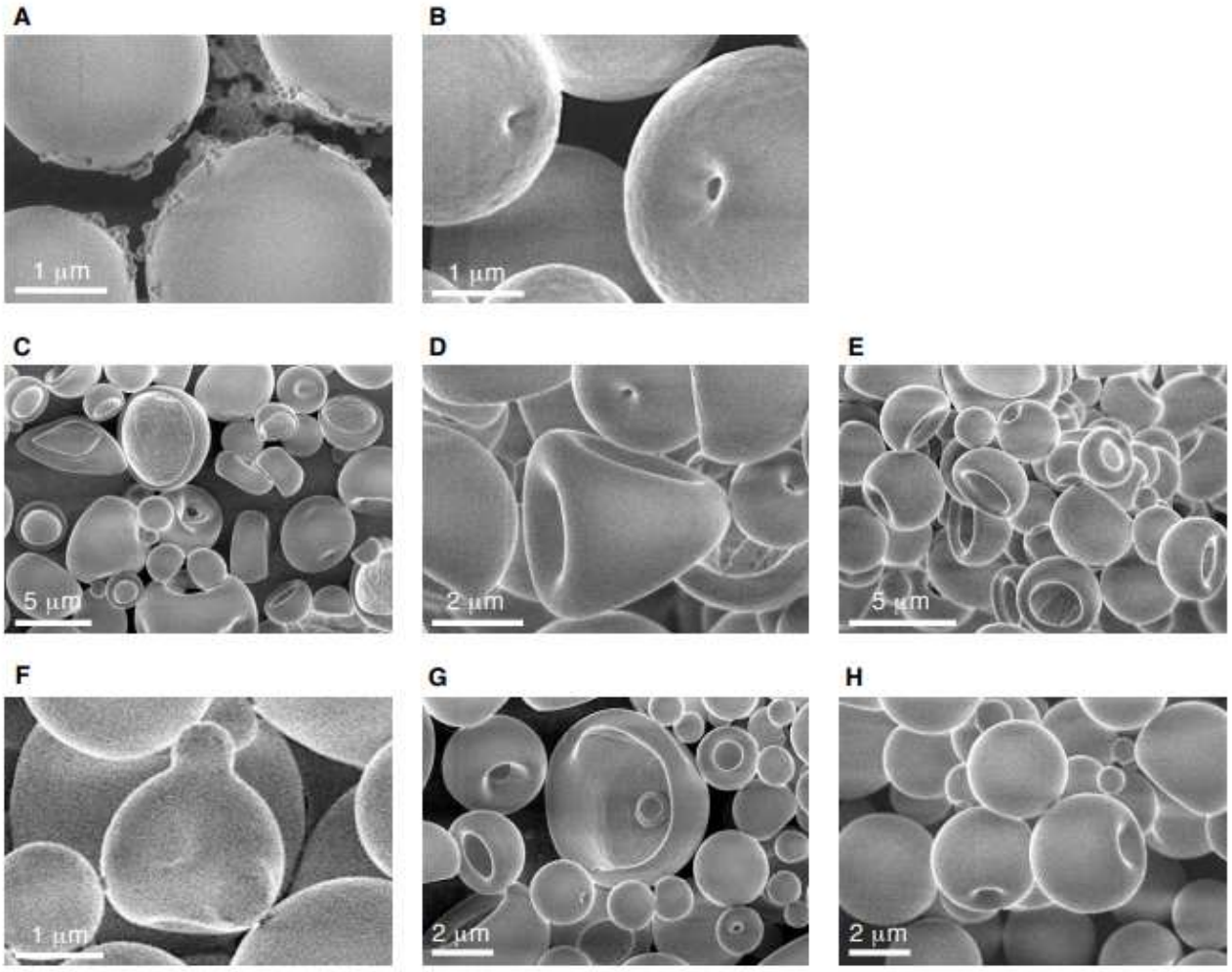

Figure 5

Effect of the solvent affinity on the transformation. FE-SEM images of the vesicles in the solution with the methanol content of (A) 80%, 50°C, (B) 80%, 25°C, (C) 60%, 50°C, (D) a knizocyte-like vesicle, 60%, 25°C, (E) 50%, 50°C, (F) a stomato II-acanthocyte vesicle, 50%, 50°C, (G) a torocyte-like vesicle, 50%, 50°C, (H) 40%, 50°C.

Supplementary Files

This is a list of supplementary files associated with this preprint. Click to download.

- SupplementaryInformationSR.pdf